PARTICLE-ROTOR DESCRIPTIONS OF ODD MASS Tl, Au, Ir ISOTOPES

Ch. Vieu*, S.E. Larsson**, G. Leander**, I. Ragnarsson**, W.de Wieclawik*** and J.S.Dionisio*

* C.S.N.S.M. (IN2P3) Lab. Salomon Rosenblum, 91406 Campus Orsay, FRANCE

** Lund Institute of Technology (Dep. Math. Phys.) LUND 7, SWEDEN

*** I.P.N. (Div. Phys. Nucl.) 91406, ORSAY, FRANCE

Abstract. Extensive asymmetric rotor model calculations were applied to the odd mass Tl, Au and Ir isotopes in order to test the ability of this model to account for the observed negative parity systems of levels and electromagnetic properties. The ε_2 quadrupole deformation of the core is derived from the potential energy curves and the γ deformation is the only free parameter. Preliminary results including the configuration mixing between different states are also quoted for ^{193,195}Au positive parity states.

1. Introduction

Several particle-rotor model calculations were recently made for the negative parity states of odd mass thallium, gold and iridium isotopes [1-4]. However, most of these calculations are not extensive enough to enable a detailed analysis of all the experimental data (level spectra and electromagnetic properties) recently collected on these isotopes [5-18]. For instance, the particle asymmetric-rotor calculations made by Meyer-ter-Vehn [2] for the odd mass gold isotopes concern mainly the ^{195}Au negative parity levels. However, there are many more accurate experimental data on ^{193}Au [11] than ^{195}Au. Consequently the former isotope is a better test for the nuclear model predictions. Similarly the Toki-Faessler calculations [3], dealing with the negative parity states of the same isotopes, concern only the high spins "yrast states". However, it is well known that the "side bands" are a more sensitive test of the nuclear model theoretical predictions. Finally there is not yet any particle asymmetric rotor calculations for the positive parity states of the Au isotopes.

In the present study an extended version of the Hecht-Satchler model [19] is applied for such purpose. From the comparison between the theoretical and the most complete $h_{9/2}$ and $h_{11/2}$ experimental systems of levels in odd mass Tl, Au and Ir isotopes, the degree of purity of the different (main K) rotational bands are deduced and the variations of the nuclear properties with the neutron number are analysed. Moreover, a theoretical interpretation of the ^{193,195}Au positive parity states is proposed using a version of the asymmetric rotor model which includes the mixing between different single proton states.

2. The particle plus triaxial rotor model

In this model, a single nucleon moves under the influence of an axially asymmetric potential ($\gamma \neq 0$) created by the core. The corresponding total Hamiltonian is a sum of the modified oscillator [20] and the triaxial rotor [19] Hamiltonian.

$$H = H_{sp} + H_{rot}$$

The single particle Hamiltonian, H_{sp}, takes into account configuration admixtures between different particle states (labelled by ν) :

$$\chi_\nu = \sum_{\alpha j \Omega} c^{(\nu)}_{\alpha j \Omega} \; \psi^{\alpha j}_{\Omega} \qquad \alpha = N, \ell$$

where $\psi^{\alpha j}_{\Omega}$ are eigenfunctions of j^2 and j_z. In the $\gamma \neq 0$ case, Ω is not a good quantum number and the single particle eigenfunctions contain components of Ω, $\Omega+2$, ...

$$\psi^{I\nu}_{MK} = \sqrt{\frac{2I+1}{16\pi^2}} \; x$$

$$\sum_{\alpha j \Omega} c^{(\nu)}_{\alpha j \Omega} \{ \mathcal{D}^I_{MK} \; \psi^{\alpha j}_{\Omega} + (-)^{I-j} \mathcal{D}^I_{M-K} \; \psi^{\alpha j}_{-\Omega} \}$$

The amplitudes $c^{(\nu)}_{\alpha j \Omega}$ are determined by solving the single particle problem with the proton shell parameters κ, μ taken from ref. 20. The ε_2 quadrupole deformation parameter is derived from the minimum of the potential energy curves [21]. The γ deformation is the only free parameter in these calculations.

In the adiabatic approximation, the rotational Hamiltonian

$$H_{rot} = \frac{\hbar^2}{2\mathcal{J}_o} \sum_{k=1}^{3} \frac{3}{4.\sin^2(\gamma + k\frac{2\pi}{3})} (I_k - j_k)^2$$

is exactly diagonalized in the set of the basis functions $\psi^{I\nu}_{MK}$ and the rotational eigenfunctions have the form :

$$\psi^I_M = \sum_{K,\nu} a^{I\nu}_K \; \psi^{I\nu}_{MK}$$

where the $a^{I\nu}_K$ coefficients are the band mixing parameters.

The B(M1) and B(E2) reduced transition probabilities were calculated in the model [22] from the rotational wave functions. The relative γ transition rates and the Δ mixing ratios were deduced from these B(σL) values and the relations.

$$\frac{I_{\gamma_1}}{I_{\gamma_2}} = \frac{B(E2)_1}{B(E2)_2} \; x \left(\frac{E_{\gamma_2}}{E_{\gamma_1}} \right)^5$$

$$1/\Delta = 1 + \frac{B(M1)}{B(E2)} \; x \; \frac{1.41 \; 10^6}{(E\gamma)^2}$$

where B(M1), B(E2) and E_γ are expressed in units of $(n.m)^2$, $(e.b)^2$ and keV respectively. In these calculations, the γ parameter is adjusted to achieve the best fitting with the experimental data (both level spectra and electromagnetic properties).

TABLE 1 : Some experimental and theoretical electromagnetic properties in Tl, Au and Ir $h9/2^-$ systems.

Nucleus	Initial state	Final state	BM1 $(n.m.)^2$ IPAR	BE2 $(eb)^2$ IPAR	Relative γ transition rates IPAR	Relative γ transition rates Exp.	Δ mixing ratios IPAR	Δ mixing ratios Exp.
^{193}Tl	$13/2_1$	$9/2_1$	-	0.013	1	1	1.0	1.0
	"	$11/2_1$	0.202	0.283	5.78	0.70 ± 0.13	0.12	$0.2^{+0.4}_{-0.8}$
	$15/2_1$	$11/2_1$	-	0.028	1	1	1.0	-
	"	$13/2_1$	0.118	0.305	1.78	0.65 ± 0.13	0.24	0.39 ± 0.28
	$17/2_1$	$13/2_1$	-	0.049	1	1	1.0	-
	"	$15/2_1$	0.298	0.297	1.88	0.4 ± 0.1	0.13	-
^{189}Au	$11/2_1$	$9/2_1$	0.052	0.006	1	1	0.01	$0.19^{+0.28}_{-0.19}$
	"	$13/2_1$	0.062	0.297	0.00	-	6.7(-3)	-
	$7/2_1$	$9/2_1$	0.067	0.405	4.29	1.0 ± 0.2	0.41	$0.13^{+0.27}_{-0.13}$
	"	$5/2_1$	0.104	0.000	1	1	1.1(-4)	$0.04^{+0.19}_{-0.04}$
^{193}Au	$9/2_2$	$9/2_1$	0.005	0.080	8.33	0.39 ± 0.13	0.85	1.0
	"	$11/2_1$	0.014	0.114	1	1	0.50	0.61 ± 0.16
	$11/2_2$	$9/2_1$	0.000	0.026	1	1	1.0	1.0
	"	$11/2_1$	0.003	0.128	0.88	1.4 ± 0.7	0.94	1.0
^{187}Ir	$7/2_1$	$9/2_1$	0.029	0.629	3.53	0.20 ± 0.03	0.37	1.0 ± 0.1
	"	$5/2_1$	0.020	0.002	1	1	2.1(-3)	≤ 0.25
	$11/2_1$	$9/2_1$	0.023	0.003	1	1	4.3(-3)	≤ 0.13
	"	$13/2_1$	0.028	0.444	0.03	0.12 ± 0.03	-	-
	$9/2_2$	$9/2_1$	0.019	0.191	5.39	-	-	-
	"	$7/2_1$	0.258	0.092	4.31	2.3 ± 1.4	-	-
	"	$11/2_1$	0.090	0.717	1	1	-	-
	$15/2_1$	$13/2_1$	0.041	0.025	1	1	-	-
	"	$11/2_1$	-	0.972	0.24	0.23 ± 0.11	-	-
	$19/2_1$	$15/2_1$	-	0.976	1	1	-	-
	"	$17/2_1$	0.043	0.084	0.31	4.7 ± 1.3	-	-

3. Odd mass thallium isotopes

The systematic occurence of a negative parity system of levels based on the first $9/2^-$ state in $^{193-199}$Tl [5,6] is well accounted theoretically by coupling the [505] 9/2 proton state with the same ε_2=-0.10 $\gamma = 18°$ asymmetric core. The adopted ε_2 value is deduced from the potential energy curves [21]. Moreover, for γ deformations close to 20 degrees, the asymmetric rotor model predicts a strongly coupled $2K = 9$ rotational band and a pair of close $13/2^-$ levels as experimentally observed (fig.3). The best fitting between the theoretical and experimental level schemes and electromagnetic properties is obtained for $\gamma = 18°$ (see fig.1 and table 1). Under these circumstances, the single proton state giving rise to the 9/2 rotational system, is mainly (98%) the $1h_{9/2\ 5/2}$ particle state with very weak admixtures of the $1h_{9/2\ 5/2}$, $2f_{5/2\ 5/2}$ and $1h_{11/2\ 9/2}$ configurations. The theoretical $h_{9/2}$ system of levels includes nearly pure $2K = 5,9$ and 13 rotational bands. Among these, the very regular $2K = 9$ band can be identified up to the $17/2^-$ level in ^{193}Tl. The identification of the higher spin members of this band can be performed using the new ^{197}Tl experimental results ($19/2^-$ at 1817 keV exp. and 2117 keV th ; $21/2^-$ 1989 exp. and 2660 keV th ; $23/2^-$ 2252 exp. and 3245 keV th ; $25/2^-$ 2458 exp. and 3874 keV th [7]. The increasing differences between the experimental and theoretical energies for high spin states reflect the softness of the core which looses its rigid character (no rotation-vibration interaction is included in the present calculation). Another reason might be the coupling to particle degrees of freedom. Finally, the theoretical static moments of the $2K = 9$ band head are $Q = -1.53$ eb and $\mu = 0.766$ n.m. They have the same order of magnitude as the corresponding theoretical moments calculated by Meyer-ter-Vehn [1] using the β and γ deformations of the neighbouring even-even mercury. In the present calculation, evidences are given that the main odd thallium nuclear properties can be attributed to the [505] 9/2 state. However, other

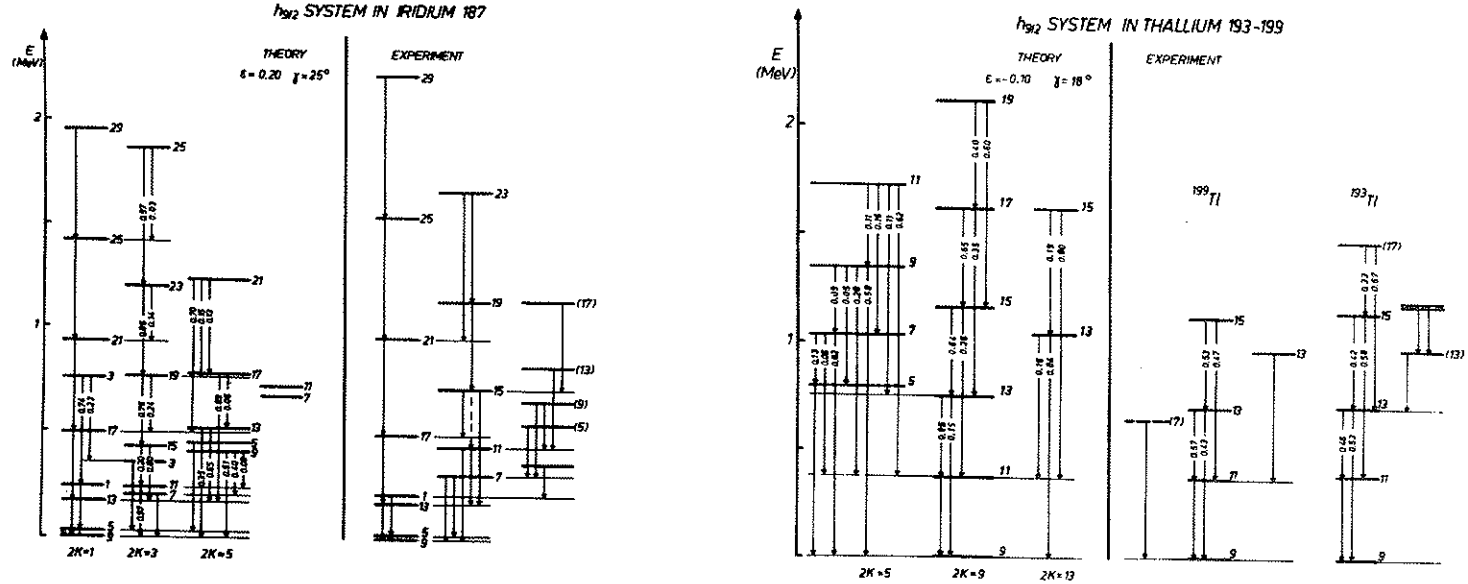

Fig. 1 Theoretical and experimental $h_{9/2}$ systems in $^{193-199}$Tl and ^{187}Ir.

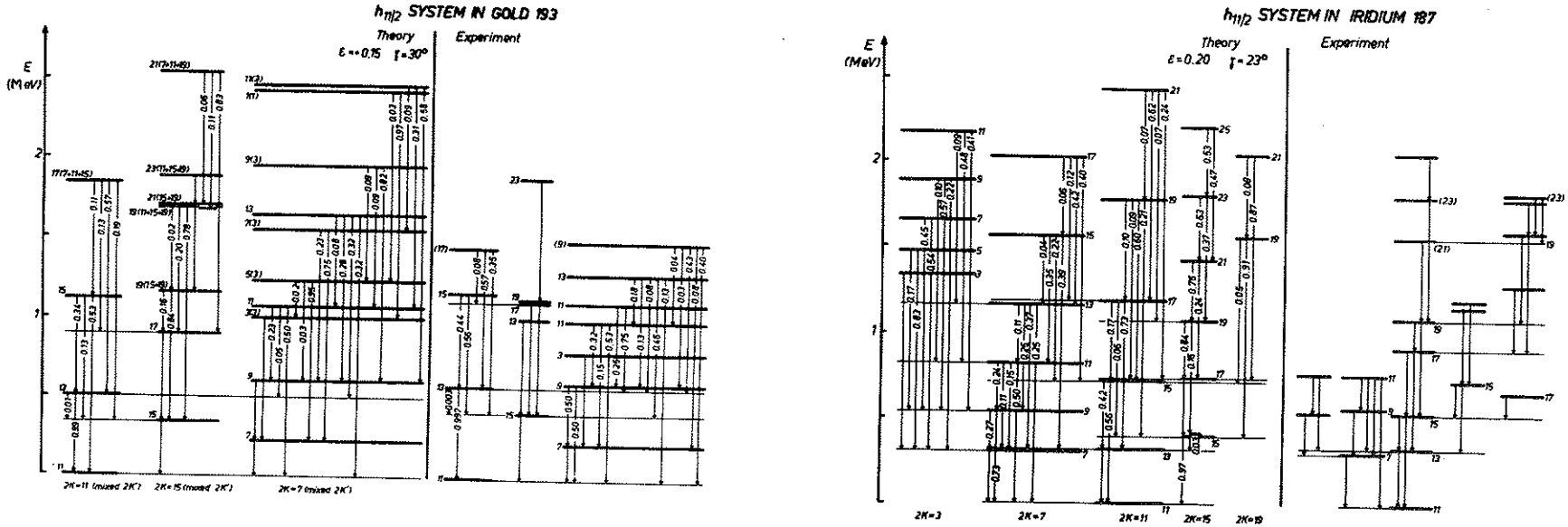

Fig. 2 Theoretical and experimental $h_{11/2}$ systems in ^{193}Au and ^{187}Ir

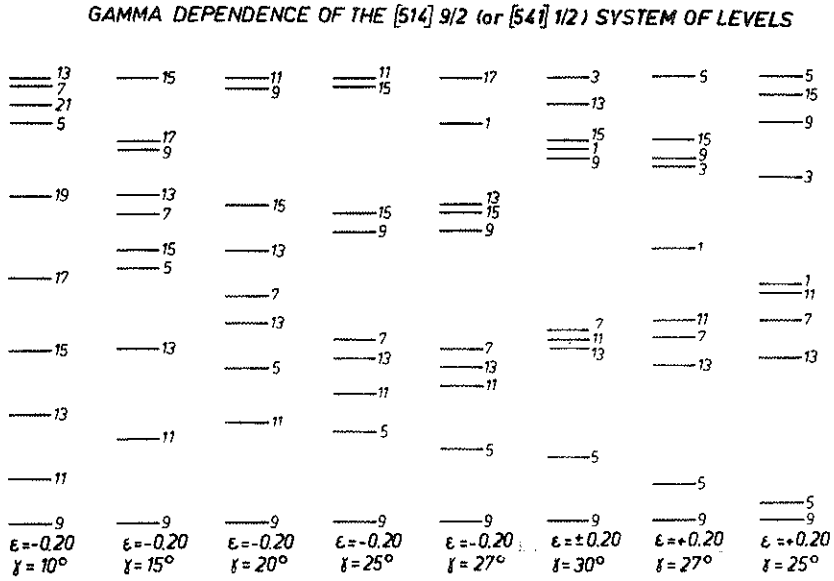

Fig.3 Gamma dependance of the theoretical $h_{9/2}$ system of levels.

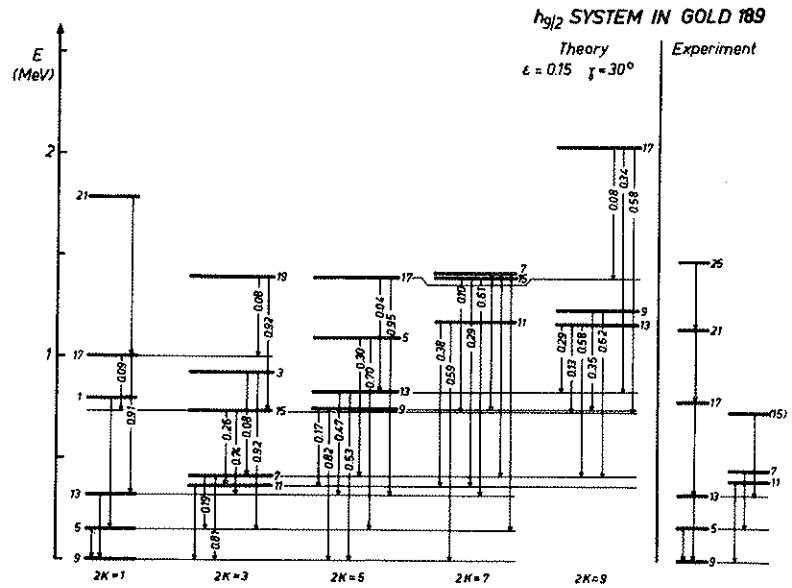

Fig.4 Theoretical and experimental $h_{9/2}$ system in ^{189}Au.

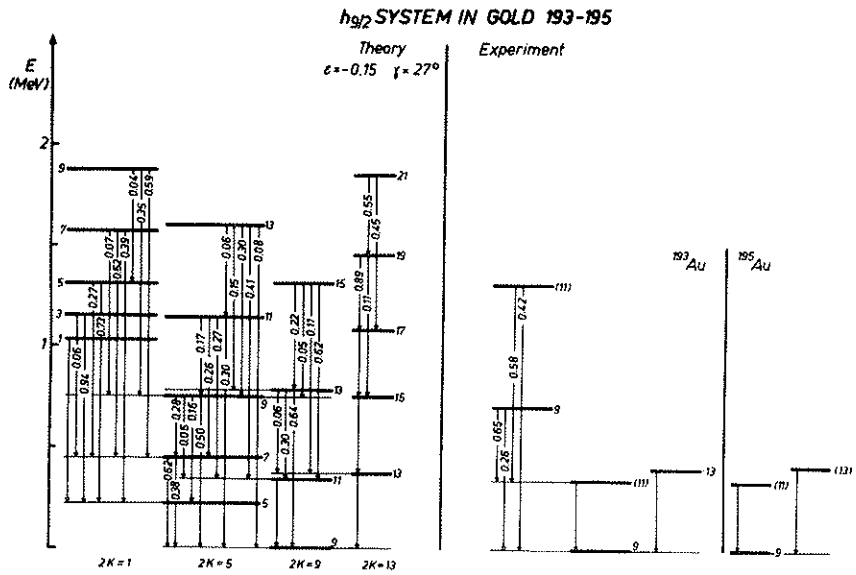

Fig.5 Theoretical and experimental $h_{9/2}$ system of levels in ^{193,195}Au.

TABLE 2 : Some experimental and theoretical electromagnetic properties in Au and Ir $h_{11/2}$ systems.

Nucleus	Initial state	Final state	BM1 $(n.m.)^2$ IPAR	BE2 $(eb)^2$ IPAR	Relative γ transition rates IPAR	Relative γ transition rates Exp.	Δ mixing ratios IPAR	Δ mixing ratios Exp.
^{193}Au	$7/2_1$	$11/2_1$	-	0.21	-	-	1.0	1.0
	$13/2_1$	$11/2_1$	0.126	0.559	173	358 ± 123	0.44	0.49 ± 0.14
	"	$15/2_1$	0.035	0.307	1	1	0.14	≤ 0.39
	$9/2_1$	$11/2_1$	0.014	0.210	1	1	0.79	0.66 ± 0.15
	"	$7/2_1$	0.158	0.611	0.87	1.0 ± 0.3	0.28	0.20 ± 0.20
	$11/2_2$	$11/2_1$	0.005	0.115	1	1	0.94	1.0
	"	$7/2_1$	-	0.163	0.44	0.46 ± 0.20	1.0	-
	"	$13/2_1$	0.026	0.200	0.11	-	0.63	-
	"	$9/2_1$	0.425	0.509	0.45	1.6 ± 0.4	0.16	0.26 ± 0.14
	$15/2_2$	$11/2_1$	-	0.134	1.58	-	1.0	-
	"	$15/2_1$	0.012	0.179	0.39	1.27 ± 0.63	0.86	(1.0)
	"	$13/2_1$	0.326	0.472	1	1	0.28	0.57 ± 0.37
	$13/2_2$	$11/2_1$	0.000	0.033	1	1	0.99	0.7 ± 0.3
	"	$15/2_1$	0.000	0.000	0.00	3.5 ± 0.9	-	1.0
	"	$13/2_1$	0.012	0.195	1.00	0.6 ± 0.2	0.93	0.66 ± 0.22
	"	$9/2_1$	-	0.281	0.89	1.0 ± 0.4	1.0	1.0
	"	$11/2_2$	0.277	0.356	0.24	1.4 ± 0.5	0.23	0.00
	$17/2_2$	$15/2_1$	0.000	0.041	0.32	0.62 ± 0.20	1.0	1.0
	"	$13/2_1$	-	0.222	1	1	1.0	1.0
	"	$17/2_1$	0.023	0.262	0.22	0.14 ± 0.05	0.88	0.51 ± 0.22
	"	$15/2_2$	0.222	0.360	0.20	-	0.37	-
^{187}Ir	$7/2_1$	$11/2_1$	-	0.237	-	-	1.0	1.0
	$15/2_2$	$11/2_1$	-	0.259	1.35	0.87 ± 0.22	1.0	-
	"	$13/2_1$	0.300	0.876	1	1	0.25	≤ 0.3
	$11/2_2$	$11/2_1$	0.002	0.090	1	1	0.96	-
	"	$7/2_1$	-	0.283	0.29	0.33 ± 0.13	1.0	-
	"	$13/2_1$	0.009	0.205	0.24	0.28 ± 0.13	0.81	-
	"	$9/2_1$	0.441	1.106	0.48	0.40 ± 0.20	0.13	-
	$17/2_2$	$13/2_1$	-	0.413	1	1	1.0	-
	"	$15/2_1$	0.000	0.050	0.08	-	1.0	-
	"	$15/2_2$	0.207	0.801	0.24	5.4 ± 1.2	0.38	-
	"	$17/2_1$	0.019	0.354	0.04	-	0.72	-

polarization effects of the core may be obtained if the influence of the neighbouring [514]7/2 and [503]7/2 single particle states were taken into account.

4. Odd mass gold isotopes

4.1. Negative parity states.

Radioactive measurements and heavy ion reaction studies, carried out on different odd mass gold isotopes, brought into evidence two systems of negative parity states based on the $11/2^-_1$ isomeric level and the $9/2^-_1$ excited state [8,13]. The $11/2^-$ system remains practically identical for all the gold isotopes. On the contrary, sharper variations of the excitation energies with the neutron number are observed for the $9/2^-$ system [9]. These two systems and their different behaviour are satisfactorily accounted by the asymmetric rotor model as shown in the present study of the most complete and significant ^{189}Au and ^{193}Au negative parity level schemes.

4.1.1. The $h_{11/2}$ systems

From the analysis of the potential energy curves [21], a low lying $11/2^-$ rotational level may arise in $^{189-195}$Au either from the [505]11/2 state with $0.1 \leqslant \varepsilon_2 \leqslant 0.2$ or from the [550]1/2 state with $-0.2 \leqslant \varepsilon_2 \leqslant -0.1$. Indeed, the energy difference between the two minima ($|V_{po}| \leqslant 0.25$ MeV) is small and no clear evidence is given for a definite prolate or oblate shape of

the core for the odd mass gold isotopes with A ⩾ 189 [21]. The best agreement between the very similar $^{189-195}$Au experimental $11/2^-$ systems and the theoretical level scheme predicted by the asymmetric rotor model is obtained for $\gamma = 30°$ (fig.2). In this way, the $BE2(7/2_1^- \rightarrow 11/2_1^-) = 0.21\ e^2b^2$ theoretical reduced transition probability is close to the corresponding experimental values ($0.36 + 0.18/-0.08$ in ^{189}Au ; 0.31 ± 0.04 in ^{193}Au). Moreover, a satisfactory agreement is also obtained between the theoretical and the most complete ^{193}Au experimental relative gamma transition rates and Δ mixing ratios (table 2)

The theoretical static moments of the $11/2_1^-$ level ($Q = 2.32$ eb ; $\mu = 3.76$ n.m.) are similar to those calculated by Meyer-Vehn [1]. Furthermore, in spite of the fact that the $h_{11/2}$ system is based on a nearly pure (97%) $h_{11/2\ 1/2}$ configuration, the higher excited states are strongly K admixted apart the first members of the $2K = 11, 15, 17$ rotational bands. Consequently, the band structures are unclear for the high spin states where intraband and interband transitions compete. Finally, these rigid rotor model calculations cannot account satisfactorily for the more compressed higher part of the experimental level scheme.

4.1.2. The $h_{9/2}$ systems

A well developped and strongly feeded $9/2^-$ system of levels with decoupled band character was established in ^{189}Au [8,9]. In the heavier odd mass gold isotopes this $9/2^-$ system has increasing excitation energies with the neutron number but its feeding decreases. Moreover, a permutation in the order of the very close $11/2_1^-$ and $13/2_1^-$ members is observed in the heavier odd mass gold isotopes [11,12]. All these experimental facts reflect a less stable character of the $9/2^-$ system in odd mass gold isotopes compared to the thallium isotopes. Indeed, a shape transition is predicted in ^{189}Au where the minimum of the [505]9/2 and the [541]1/2 potential energy curves have the same energy [21]. The best agreement between the ^{189}Au experimental and theoretical results is obtained by coupling the [541]1/2 particle state to an asymmetric core with $\varepsilon_2 = 0.15$ and $\gamma = 30°$ deformations (fig.4). In this way, the experimental $9/2_1^-$, $5/2_1^-$, $13/2_1^-$, $17/2_1^-$ and $11/2_1^-$, $7/2_1^-$, $15/2_1^-$ levels are identified to the members of the $2K = 1$ and $2K = 3$ decoupled bands respectively. These bands are partly mixed which explains the deexcitation of the $15/2_1^-$ ($2K = 3$) level towards the $13/2_1^-$ ($2K = 1$) lower state. This increasing influence of the rotation-vibration interaction in the high spin states appears clearly from the comparison between the experimental and the theoretical excitation energies of the $21/2^-$ (at 1336.7 keV exp. and 1780 keV th.) and $25/2^-$ (at 1973.7 and 2654 keV) members of the $2K = 1$ rotational band. Among the few available ^{189}Au experimental electromagnetic properties, the $BE2(5/2_1^- \rightarrow 9/2_1^-) = 0.84 \pm 0.08$ e^2b^2 reduced transition probability agrees with the corresponding theoretical value (see table 1).

In the heavier odd mass gold isotopes, the experimental results are more scattered. However, the permutation of the $11/2_1^-$ and $13/2_1^-$ levels, the experimental relative gamma transition rates and the Δ mixing ratios are well accounted theoretically by coupling the [505]9/2 particle state to an oblate core with $\varepsilon_2 = 0.15$ and $\gamma = 27°$ deformations (see fig.5 and table 1). The single proton state giving rise to the ^{189}Au $9/2^-$ system is much more complex than in ^{193}Au. Indeed, its wave function has a main (64%) $h_{9/2\ 1/2}$ component but it receives also (26% and 6%) contributions from the $h_{9/2\ 3/2}$ and $h_{9/2\ 5/2}$ configurations. On the contrary, the ^{193}Au single proton state is identified to the nearly pure (93%) $h_{9/2\ 9/2}$ configuration. For both isotopes, the $h_{9/2}$ and $h_{11/2}$ systems of levels arise from a particle and hole state which have wave functions with negligible overlap. Having in mind that these two negative parity systems of levels correspond to different core shapes, both facts explain the observed hindrance factors of the $9/2_1^-(h_{9/2}$ system) $\rightarrow 11/2_1^-(h_{11/2}$ system) transitions in gold 189 and 193 [9].

4.2 Positive parity states.

In the odd mass gold isotopes, the positive parity states form a relatively stable pattern [8-13].

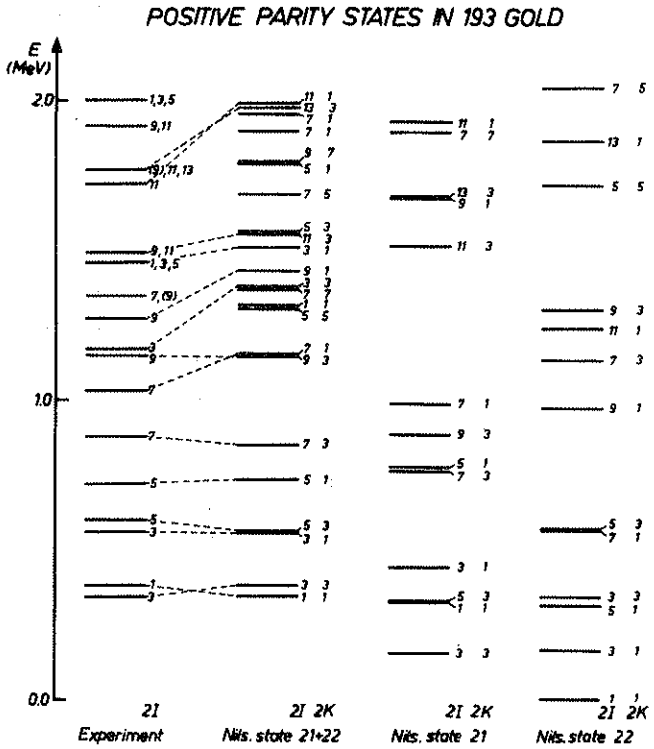

Fig.6 - Comparison between the ^{193}Au experimental positive parity states and the theoretical spectra obtained by coupling the proton states 21 (55 % $2d_{3/2\ 3/2}$ + 26% $3s_{1/2\ 1/2}$) and 22 (41% $3s_{1/2\ 1/2}$ + 35% $2d_{3/2\ 3/2}$) to an asymmetric ($\varepsilon_2 = 0.15$; $\gamma = 20°$) core. The two theoretical level schemes indicated on the right correspond to the unperturbed systems based on the proton hole states 21 or 22. The relative positions of these theoretical systems are in arbitrary units.

The analysis of the experimental data and the existence of characteristic 3/2, 5/2, 7/2, 9/2 and 11/2 interconnected doublet levels deexciting towards the $3/2_1^+$ and $1/2_1^+$ states give arguments for a possible rotational system based on these two levels. This conclusion is supported theoretically by the identification of the $3/2_1^+$ and $1/2_1^+$ levels to the [402]3/2 and [400]1/2 neighbouring proton hole states on account of their relative position to the Fermi level. The potential energy curves do not indicate any clear prolate or oblate deformation for these two states [21]. However, the asymmetric rotor model predicts $3/2^+$ and $1/2^+$ rotational systems including the observed doublets for $\varepsilon_2 = 0.15$ and $\gamma = 20°$ deformations (fig.6). On account of their very similar static wave functions, one cannot neglect their mixing in these asymmetric rotor model calculations. This was done in the present study and the overall agreement between the experimental and theoretical level schemes confirms the predominant role of the $2d_{3/2}$ and $3s_{1/2}$ shells in the low and medium energy positive parity states.

This mixed $3/2^+ + 1/2^+$ character of the positive parity states in the odd mass gold isotopes generally smoothes the characteristic electromagnetic properties commonly used for the identification of a pure rotational band.

5. Odd mass iridium isotopes

Among the odd mass iridium isotopes, the most complete experimental results were obtained in ^{187}Ir and ^{189}Ir [14-18]. They gave evidence for complex $h_{11/2}$ and $h_{9/2}$ systems of levels less stable with the neutron number than those observed in odd mass gold and thallium isotopes respectively. The present theoretical analysis is carried out for ^{187}Ir but remains valid for ^{189}Ir. However, it cannot be applied to the heavier odd mass iridium isotopes where both the experimental data and the potential energy curves predicts shape transitions for the $h_{11/2}$ and $h_{9/2}$ systems.

5.1. The ^{187}Ir $h_{11/2}$ system

The experimental $h_{11/2}$ system includes two strongly coupled rotational bands based on the $11/2_1^-$(434.0 keV) isomeric state and the $7/2_1^-$(738.6 keV) level (see fig.2). Other less developped and complex bands exist which are built on the $15/2^-$ (1159.4 keV) and $19/2^-$ (2034.0 keV). However, their theoretical analysis cannot be performed until now due to the lack of precise spectroscopic measurements. A general good agreement can be obtained between the experimental and theoretical K = 11/2 and 7/2 bands by coupling the [505]11/2 proton hole state to an $\varepsilon_2 = 0.20$, $\gamma = 23°$ asymmetric core. Similar fit can be obtained in ^{189}Ir if the γ deformation is increased up to 25°. The adopted $^{187\text{-}189}$Ir quadrupole deformation is slightly higher than the theoretical (0.16, 0.17) values deduced from the potential energy curves [21]. However, it accounts satisfactorily for the observed gamma transition rates and the experimental $BE2(7/2_1^- \rightarrow 11/2_1^-) = 0.31 \pm 0.03\ e^2b^2$ reduced transition probability measured in ^{189}Ir (table 2).

The analysis of the experimental and theoretical ^{187}Ir results shows that the different K rotational bands are in general complex. Indeed, they arise from a proton hole state whose wave function includes 48% 32% and 14% contributions from the $h_{11/2\ 1/2}$ $h_{11/2\ 3/2}$ and $h_{11/2\ 5/2}$ configurations respectively. In this way, the $11/2_1^-$ and $13/2_1^-$ levels are the only ones which are practically 2K = 11 pure rotational states. The $15/2_1^-$ and $17/2_1^-$ members of the same band have noticeable 2K = 15 and 2K = 7 components in their wave functions. Finally, the $19/2_1^-$ and $21/2_1^-$ levels with streched E2 transitions towards the lower 2K =11 rotational states have no main 2K=11 component but receive nearly the same contribution from the 2K=7, 11,15 and 19 bands. A similar analysis of the 2K=7 band shows that all its members with spin values higher than 15/2 receive noticeable contributions from 2K=3 and 11 bands. This explains the observed interband transitions deexciting these high spin states where the K mixing is important.

5.2. The ^{187}Ir $h_{9/2}$ system

Two well developped rotational bands based on the $9/2_1^-$ (186.2 keV) and $7/2_1^-$ (486.5 keV) levels are observed in ^{187}Ir [15-16]. These levels and their electromagnetic properties are well accounted theoretically by coupling the [541]1/2 particle state with a $\varepsilon_2 = 0.20$, $\gamma = 25°$ asymmetric core (see fig.1 and table 1). In this way the wave function has a main (66%) $h_{9/2\ 1/2}$ component but receives also 21%, 6% and 4% contributions from the $h_{9/2\ 3/2}$, $f_{5/2\ 3/2}$ and $h_{9/2\ 5/2}$ configurations.

The 2K = 1 rotational band includes a remarkable sequence of levels which are identified experimentally up to the $I=29/2^-$ (2401.0 keV) and $I=33/2^-$ (3151.8 keV) states. It receives noticeable 2K = 3 and 2K = 5 admixtures. However, due to the fact that the neighbouring rotational levels are higher in energy, only the intense 2K = 1 intraband transitions can occur. Similar K admixtures exist in the 2K = 3 rotational band based on the $7/2_1^-$ level. It explains the 2K = 3 → 2K = 1 interband transitions which compete with intraband transitions. Due to higher K mixing, the elements of the 2K = 5 and 2K = 7 bands have very complex desexcitation modes making the identification of their different elements very puzzling. Finally, the $h_{9/2}$ system in ^{189}Ir is well described with a $\gamma = 27°$ deformation slightly higher than the adopted value for ^{187}Ir. Similar fact was precedently noticed for ^{187,189}Ir $h_{11/2}$ systems.

6 - Conclusions

The present study shows that many valuable tests of the asymmetric rotor model can be derived from a detailed analysis of all the available nuclear properties of low, medium and high excited states in Tl, Au and Ir odd mass isotopes. This explains the great interest of extensive and precise spectrometry measurements in all these transitional nuclei.

Satisfactory theoretical descriptions were obtained for the negative parity states using the asymmetric rotor model and the ε_2, γ deformations deduced from the potential energy curves and the comparison between experimental and theoretical results. A part from the pure and stable $h_{9/2}$ rotational bands in thallium isotopes, the observed $h_{9/2}$ and $h_{11/2}$ systems in gold and iridium isotopes are K mixed in general. This K mixing becomes particularly important for γ deformations higher than 20 degrees but does not seem strongly related to the more or less complex character of the single-particle levels on which the rotational bands are based (see the ^{193}Au and ^{187}Ir $h_{11/2}$ systems).

As far as the positive-parity states are concerned the agreement is satisfactory for these preliminary results.

REFERENCES

1. J. Meyer-ter-Vehn, F.S. Sthephens and R.M. Diamond, Phys. Rev. Lett. 32 (1974) 1383.
2. J. Meyer-ter-Vehn, Nucl. Phys. A249 (1975) 111
3. H. Toki and A. Faessler, Nucl. Phys. A253 (1975) 231.
4. K.T. Hecht, Phys. Lett. 58B n°3 (1975) 253
5. J.O. Newton, F.S. Stephens and R.M. Diamond, Nucl. Phys. A236 (1974) 225.
6. J.O. Newton, S.D. Cerilov, F.S. Stephens and R.M. Diamond, Nucl. Phys. A148 (1970) 593
7. R.M. Lieder, M. Müller-Veggian, Y. Gono, A. Neskakis, C. Mayer-Böriche, S. Beshai, K. Fransson, C.G. Lindén and Th. Lindblad, Annual Report (1975) Research Institute for Physics, Stockholm.
8. V. Berg, R. Foucher and Å Höglund, Nucl. Phys. A244 (1975) 462.
9. V. Berg, C. Bourgeois and R. Foucher, Journ. Phys. 36 (1975) 613.
10. M.A. Deleplanque, C. Gerschel, N. Perrin and V. Berg, Nucl. Phys. A249 (1975) 366.
11. Ch. Vieu, thesis, University of Paris, Orsay 1974
12. Ch. Vieu, A. Peghaire and J.S. Dionisio, Rev. Phys. Appl. 8 (1973) 231.
13. E.F. Zganjar, J.L. Wood, R.W. Fink, L.L. Riedinger, C.R. Bingham, B.D. Kern, J.L. Weil, J.H. Hamilton, A.V. Ramayya, E.H. Spejewski, R.L. Mlekodaj, H.K. Carter and W.D. Schmidt-Ott, Phys. Lett. 58B N°2 (1975) 159.
14. C. Sebille-Schück, M. Finger, R. Foucher, J.P. Husson, J. Jastrzebski, V. Berg, S.G. Malmskog, G. Astner, B.R. Erdal, P. Patzelt and P. Siffert, Nucl. Phys. A212 (1973) 45.
15. S. André, J. Boutet, J. Rivier, J. Tréherne, J. J. Jastrzebski, J. Lukasiak, Z. Sujkowski and C. Sebille-Schück, Nucl. Phys. A243 (1975) 229.
16. P. Kemnitz, L. Funke, H. Sodan, E. Will and G. Winter, Nucl. Phys. A245 (1975) 221.
17. A. Bäcklin, V. Berg and S.G. Malmskog, Nucl. Phys. A156 (1970) 647.
18. R.H. Price, D.G. Burke and M.W. Johns, Nucl. Phys. A176 (1971) 338.
19. K.T. Hecht and G.R. Satchler, Nucl.Phys. 32 (1962) 286.
20. S.G. Nilsson, C.F. Tsang, A. Sobiezewski, Z. Szymanski, S. Wycech, C. Gustafson, I.L. Lamm, P. Möller and B. Nilsson, Nucl. Phys. A131 (1969) 1.
21. W. de Wieclawik, I. Ragnarsson, S.E. Larsson, G. Leander, Ch. Vieu and J.S. Dionisio, communication to the present Conference.
22. S.E. Larsson, G. Leander, I. Ragnarsson, to be published.